Journal of Materials Chemistry B

Accepted Manuscript

ROYAL SOCIETY OF CHEMISTRY

www.rsc.org/materialsB

Journal Name

ARTICLE

Development of itraconazole encapsulated polymeric nanoparticle platform for effective antifungal therapy

Received 00th January 20xx,
Accepted 00th January 20xx

DOI: 10.1039/x0xx00000x

www.rsc.org/

Xiang Ling [a, d], Zewei Huang [b], Jianzhao Wang [a], Jiarong Xie [a], Min Feng [a], Yang Chen [c], Farhana Abbas [d], Jiasheng Tu [a, *], Jun Wu [d, *], Chunmeng Sun [a, *]

This study is to develop a novel itraconazole-loaded nanoparticle (ITZ-NP) platform for effective antifungal therapy. First, the monomethoxypoly(ethylene glycol)-b-poly(lactic acid) (mPEG-b-PLA) copolymer was prepared as drug carrier material. Then the nanoparticles were formulated via a simple film hydration method. The copolymer and nanoparticles were characterized by standard methods, including ^{1}H NMR, ^{13}C NMR, FT-NIR, DSC, XRPD, particle size, zeta potential, morphology and physical examination. Furthermore, *in vitro* itraconazole release and antifungal activity were intensively evaluated. The results showed that the formed nanoparticles significantly enhanced sustained drug release and inhibited fungal infection. In addition, ITZ-NP caused very mild hemolysis and slight venous irritation, indicating much better biocompatibility than marketed cyclodextrin formulation of ITZ. *In vivo* biodistribution study via intravenous injection showed that ITZ-NP was able to be effectively retained in blood circulation and selectively distributed in RES-rich organs compared with commercial cyclodextrin injection, with the verification of Re, Te, R_{Te} and Ce. In summary, the developed ITZ-NP could reduce systemic toxicity, improve antifungal activity and act as a potential intravenous formulation of ITZ.

Introduction

As an important azole broad-spectrum antifungal agent, itraconazole (ITZ), blocking the synthesis of ergosterol on the fungal biofilms, is widely prescribed for normal and immunocompromised hosts with serious fungal infections, such as *Aspergillosis*, *Blastomyces*, *Candida*, *Cryptococcus*, disseminated *Penicillium mameffei* infections and *Histoplasma capsulatum var. capsulatum* [1-3]. Although progresses have been made by oral formulation of ITZ, parenteral administration is urgently needed for those neutropenic and other immunocompromised patients with dysphagia [4, 5]. In addition, intravenous administration with high plasma and tissue levels in a short time is vital for ITZ due to a well-defined quantitative correlation between *in vitro* MIC activity and clinical performance [6].

Nevertheless, it's challenging to develop intravenous formulations for chemical entities like ITZ due to its high lipophilicity (clog *P* = 6.2), low water solubility (*S* ~1 ng/mL at pH 7 and ~5 μg/mL at pH 1), strong alkalinity (p*K*a = 2 and 3.7), and relative large molecular weight (M = 705.64 g/mol) [7-9]. Nowadays, intravenous formulations of ITZ is only commercialized as Sporanox® i.v. (ITZ-HP-β-CD) containing inclusion complex of ITZ and hydroxypropyl-β-cyclodextin (HP-β-CD), which facilitates the establishment of high and dependable concentrations of the drug in plasma. However, Sporanox® i.v. has very limited clinical applications because of the high toxicity of HP-β-CD to patients with severe renal impairment. On the other hand, rat carcinogenicity study proved that HP-β-CD induced pancreatic adenocarcinoma [10]. Thus, a new intravenous formulation is highly needed and of great potential.

Great efforts have been devoted to develop new drug delivery systems for ITZ. Among them, polymeric nanoparticles have been promising delivery systems for water-insoluble chemical entities [11-13]. Thus, they could be the ideal candidates to deliver ITZ. For example, monomethoxypoly(ethylene glycol)-b-poly(lactic acid) (mPEG-b-PLA) copolymer, which possessed desirable biodegradability and biocompatibility, could be formulated into small nanoparticles through self-assembly. The PEG segments had widely believed to provide a long circulation effect for drugs [14]. By varying the composition of PEG and PLA, a library of nanocomposites or nanostructured biomaterials could be obtained with desired physicochemical properties and applications [15].

In the current study, ITZ-loaded mPEG-b-PLA nanoparticles (ITZ-NP) with desirable size and morphology were prepared by the film hydration method. The physicochemical characterization, *in vitro* release behavior and antifungal activity, hemolysis and injection irritation of ITZ-NP were also evaluated. Furthermore,

[a] State Key Laboratory of Natural Medicines, Department of Pharmaceutics, School of Pharmacy, China Pharmaceutical University, Nanjing 210009, China.
[b] Sichuan Institute for Food and Drug Control, Chengdu 611731, China.
[c] Department of Key Laboratory of Drug Metabolism and Pharmacokinetic, School of Pharmacy, China Pharmaceutical University, Nanjing 210009, China.
[d] Laboratory of Nanomedicine and Biomaterials, Department of Anesthesiology, Brigham and Women's Hospital, Harvard Medical School, Boston, MA 02115, USA.
*Correspondence - suncm_cpu@hotmail.com

biodistribution and pharmacokinetics were investigated in mice in comparison with ITZ-HP-β-CD.

Experimental

Materials, *Candida albicans* and animals

Itraconazole was purchased from Shouguang Fukang Pharmaceutical, China. Methoxypoly(ethylene glycol) (mPEG, M_n = 2000) was supplied by Fluka, USA. D,L-Lactide was obtained from Jinan Daigang Biomaterial, China. Stannous octoate ($Sn(Oct)_2$) was offered by Sigma-Aldrich. The cyclodextrin formulation of itraconazole (Sporanox® i.v.) was presented by Janssen Pharmaceutica of Belgium. Physiological saline was bought from Kaikaii Yuansheng Pharmaceutical, China. Dulbecco's Modified Eagle's Medium (DMEM) and fetal bovine serum (FBS) were bought from Gibco®. All other chemicals were of HPLC or analytical grade.

Candida albicans (*C. albicans*) strain ATCC 10231, the laboratory-adapted strain with less virulence in animal models, purchased from Institute of Microbiology, Chinese Academy of Science, Beijing, China, was grown on Sabouraud's Glucose Broth Medium for 24 h at 37 ℃ with a shaking rate of 100 rpm.

New Zealand rabbits and ICR mice were provided by Laboratory Animal Research Center of Jiangsu University and College of Veterinary Medicine, Yangzhou University, respectively. Those animals were acclimatized at 22 ± 2 ℃ and 70 ± 5% relative humidity under natural light-dark conditions with access to food and water throughout all the experiments. All care and handling of animals were conducted according to the National Institute of Health Guide for the Care and Use of Laboratory Animals and approved by the Animal Ethics Committee of China Pharmaceutical University.

Synthesis of mPEG-b-PLA copolymer

mPEG-b-PLA copolymer was synthesized by ring-opening polymerization of D,L-Lactide in the present of mPEG using a monomer ratio of 40:60 [16, 17]. Briefly, calculated amounts of mPEG, D,L-Lactide and $Sn(Oct)_2$ were added into a flask under the protection of nitrogen atmosphere in advance. The mixture was maintained at 150 ℃ under mechanical stirring for 6 h. Then, the reaction system was evacuated under vacuum for another 45 min followed by being cooled to room temperature (R.T.) under nitrogen atmosphere. Finally, the crude product of mPEG-b-PLA copolymer was reprecipitated from dichloromethane with excess pre-cold anhydrous diethyl ether. The resultant precipitate was filtered and vacuum dried to constant weight. Purified mPEG-b-PLA copolymer was kept in desiccator before further use [18].

Preparation of ITZ-NP

ITZ-NP was prepared by a simple film hydration method. Firstly, equimolar amounts of ITZ and HCl were dissolved in ethanol (ITZ 10 mg/mL), and 3 mL of the obtained drug solution was added to 0.75 g of mPEG-b-PLA copolymer dissolved in appropriate amount of dichloromethane. After vortexing, solvents were removed at 55 ℃ with a rotary evaporator to form the polymer-drug film, which was then dispersed by adding 3 mL of deionized water under gentle shaking for 5 min. Afterwards, the solution was adjusted to pH 4.5, filtered through 0.22 μm microporous membrane filter to remove unincorporated drugs, and lyophilized to afford ITZ-NP. The powder was stored under 4 ℃ and could be easily redissolved in physiological saline by mild shaking before application. Drug loading (DL) and entrapment efficiency (EE) are represented by following formulas, respectively.

$$\mathrm{DL}\ (\%) = \frac{\text{ITZ weight in nanoparticles}}{\text{Total weight of nanoparticles}} \times 100$$

$$\mathrm{EE}\ (\%) = \frac{\text{ITZ weight in nanoparticles}}{\text{Feeding ITZ weight}} \times 100$$

General measurements

^{1}H NMR spectra were recorded on a Bruker AV-500 NMR Spectrometer (Switzerland) in $CDCl_3$, while ^{13}C NMR spectra were measured by Bruker AV-300 NMR Spectrometer (Switzerland) at R.T.. Fourier Transform Near Infrared (FT-NIR) spectra measurements were conducted on a Bruker TENSOR 27 spectrometer (Germany) using KBr method. Thermal behaviors were analyzed by Differential Scanning Calorimeter (DSC 204, NETZSCH Group, Germany): temperature ranged from 40 to 300 ℃, heating rate was 10.0 K/min and nitrogen purged at a speed of 20 mL/min. X-ray Powder Diffraction (XRPD) patterns were obtained with Bruker D8 Advance X-ray Diffraction Instruments (Germany) using Ni filtered Cu Kα1 radiation, an accelerating voltage of 40 kV, a beam current of 60 mA, a step size of 0.05°, and a data acquisition time of 2.0 s per step. XRPD was carried out at R.T. with a scanning speed of 4°/min between 5 and 50 2θ angle. ITZ was determined by High Performance Liquid Chromatography (HPLC, UltiMate 3000, Thermo Fisher, USA) equipped with an Agela Durashell C_{18} column (4.6 mm × 150 mm, 5 μm). The mobile phase of acetonitrile and 0.02 M tetrabutylammonium hydrogen sulfate (50:50) was run isocratically at 35 ℃ at a flow rate of 1.0 mL/min. The injection volume was 20 μL and UV detector was fixed at 263 nm.

Particle size, zeta potential and morphology

Particle size and zeta potential were measured by Particle Size & Zeta Potential Analyzer (90Plus Zeta, Brookhaven Instruments Corporation, USA). Samples were diluted with physiological saline to ensure that all the measurements were performed under conditions of enough ionic strength, in which the surface charge may be more accurate. Dynamic light scattering (DLS) mode was used to measure vesicular size and size distribution at 25 ℃ and a scattering angle 90°. Laser Doppler Velocimetry (LDV) mode was chose to determine zeta potential.

The morphology was investigated by Atomic Force Microscopy (AFM, Nano Scope IIIa, Veeco Instruments, USA). A drop of aqueous solution of ITZ-NP was placed on a clean mica surface washed with deionized water and purged with nitrogen. The samples were then dried under an argon atmosphere. Successively, the surface containing ITZ-NP was visualized by AFM in a scanned area of 0.5 μm × 0.5 μm, and particle size was also obtained using Nano Rule software. The height differences on the surface were indicated by the color code (lighter regions indicated higher heights).

Physical examination

pH: pH was measured at 25 ℃ using a IQ150 pH Meter with PH17-SS pH Electrode (Hach, USA).

Osmotic pressure (OP): Freezing point depression method (Micro-Osmometer, Model 3300, Advanced Instruments, USA) was adopted to obtain osmotic pressure.

Dilution stability: ITZ formulations were diluted with 10% FBS DMEM media at different concentrations and stored at 25 ℃ for 24 h. Color, homogeneity and phase separation were examined [19].

Drug release

In vitro release of ITZ formulations was performed as follows: 1 mL of samples (ITZ 1 mg/mL) were sealed in pre-swelled dialysis bags with 3.5 kDa MWCO, and immersed in 199 mL physiological saline containing 1% Tween 80 and 0.7% HCl at 37 ℃ with stirring at 100 rpm. At designed time intervals, sample solution (2.0 mL each) was withdrawn and quantified by HPLC. Equal volume of fresh medium was immediately replenished.

***In vitro* antifungal activity**

The sensitivity of *C. albicans* to different ITZ formulations was performed according to the reference method for broth antifungal testing (National Committee for Clinical Laboratory Standards, document M27-A2, 2002). Sabouraud's Glucose Agar and Broth Medium were sterilized by autoclaving at 15 psig pressures, 121 ℃ for 15 min. *C. albicans* were prepared in Sabouraud's Glucose Broth Medium, calculated by colony count method and diluted with fresh medium to 10^3 CFU/mL. Fresh cultures of *C. albicans* were incubated in medium tubes containing 0.0153, 0.0610, 0.2441, 0.9766, 3.9063, 15.6250, 62.5000, 250.0000 and 1000.0000 μg/mL ITZ for 2 h. Then the cultures were plated onto Sabouraud's Glucose Agar Plate, incubated at 37 ℃ for 24 h, and colony forming units were quantified. The activity of ITZ formulations was calculated as inhibition rate of *C. albicans* compared to the control (the absence of ITZ).

Red blood cells (RBCs) hemolysis

RBCs, collected from rabbit blood, were diluted with physiological saline to 2 v/v%. ITZ formulations were mixed with RBCs suspensions at gradient concentrations from 0.001 to 10 mg/mL, incubated at 37 ℃ for 3 h, centrifuged at 1500 rpm for 15 min. Supernatant was measured via Absorbance Microplate Reader (ELx800, BioTek Instruments, USA) at 541 nm, hemolysis rate was determined:

$$\text{Hemolysis rate } (\%) = \frac{A_{sample} - A_0}{A_{100} - A_0} \times 100$$

Where, A_{sample} was the absorbance of sample, A_{100} was the absorbance of lysed RBCs in deionized water (positive control), A_0 was the absorbance of 0% hemolysis in physiological saline (negative control) [20].

Injection irritation

12 New Zealand rabbits (1.8-2 kg) were randomly divided into 4 groups. ITZ formulations made at a rate of 1 mL/min were injected via left marginal ear vein for three consecutive days. Equivoluminal mPEG-b-PLA copolymer and physiological saline were given to the other two groups. Any paradoxical reactions were recorded by an experienced unbiased observer. Injection sites and proximal region were stained with hematoxylin and eosin (HE), followed by histopathological examination using an Upright Metallurgical Microscope (BX45-DP72, Olympus Corporation, Japan).

Biodistribution

A certain amount of ITZ formulations (20 mg ITZ /kg) were respectively injected into healthy ICR mice (20-22 g, 6 in each group, half male and half female). At 5 min as well as 0.25, 0.5, 1, 2, 4, 8, 12 h, plasma and organs (heart, liver, spleen, lung, kidney and brain) were harvested, and the amounts of ITZ were quantitatively measured by HPLC [21].

For the plasma, 150 μL of sample was pipetted into an Eppendorf centrifuge tube, to which 50 μL of internal standard (10 μg diazepam/mL), 50 μL of 1.5 M sodium hydroxide solution and 2 mL tert-butyl methyl ether were added and vortexed for 3 min. After the organic phase was separated and evaporated, the residue was reconstituted with 500 μL mobile phase and centrifuged before analysis. For the organs, 500 μL homogenized sample was taken for analysis and processed similarly to plasma.

Pharmacokinetics

Following analysis describe above, pharmacokinetics parameters were derived from mean plasma concentration-time curves and determined using a Phoenix WinNonlin 6.3 Program (Pharsight Cooperation, St. Louis Missouri, USA). Hence, the following parameters were obtained: the peak concentration in plasma (C_{max}), volume of distribution at steady state (V_{ss}), total body clearance (CL), the area under the plasma concentration-time curve from time zero to time infinity ($AUC_{0\rightarrow inf}$), the area under the moment plasma concentration-

time curve from time zero to time infinity ($AUMC_{0\to inf}$), mean residence time from time zero to time infinity ($MRT_{0\to inf}$). The targeting ability *in vivo* was evaluated with Re (relative uptake rate), Te (targeting efficiency), R_{Te} (relative targeting efficiency) and Ce (peak concentration ratio) [22].

$$\mathrm{Re} = \frac{(\mathrm{AUC})_{\mathrm{ITZ-NP}}}{(\mathrm{AUC})_{\mathrm{ITZ-HP-\beta-CD}}}$$

$$\mathrm{Te} = \frac{\mathrm{AUC_{target}}}{\sum(\mathrm{AUC_{target}} + \mathrm{AUC_{no-target}})} \times 100$$

$$\mathrm{R}_{Te} = \frac{(\mathrm{Te})_{\mathrm{ITZ-NP}}}{(\mathrm{Te})_{\mathrm{ITZ-HP-\beta-CD}}}$$

$$\mathrm{Ce} = \frac{(\mathrm{C_{max}})_{\mathrm{ITZ-NP}}}{(\mathrm{C_{max}})_{\mathrm{ITZ-HP-\beta-CD}}}$$

Statistical analysis

All experiments were repeated at least three times. Data were analyzed with SPSS 20.0 software and expressed as the mean ± standard deviation. Unpaired student's *t*-test was used for between two-group comparison and one-way analysis of variance (ANOVA) with LSD and S-N-K tests for multiple-group analysis (*, $p < 0.05$; **, $p < 0.01$; ***, $p < 0.001$).

Results and discussion

mPEG-b-PLA copolymer, a white solid powder synthesized by ring-opening polymerization, was characterized by ^{1}H NMR and its spectrum was displayed in Fig. 1(1). Peaks at 3.38 and 3.64 ppm corresponded to methyl (A) and methylene (B) protons of mPEG segments respectively, while chemical shifts at 1.56 and 5.17 ppm were assigned to methyl (E) and methine (D) protons of PLA segments, verifying the structure of mPEG-b-PLA copolymer. Methylene (C) protons next to PLA segments and methine (F) protons at the end of PLA segments coincided at 4.35 ppm. These data were identical with the published report and demonstrated the successful synthesis of mPEG-b-PLA copolymer [23]. From the ratio of peak areas (D:B = 1:4.57), the number average molecular weight (M_n) was very close to the theoretical number 5000, and the content of mPEG segments was around 41.16%.

As the ^{13}C NMR spectrum shown in Fig. 1(2), peaks at 58.69 and 70.27 ppm belonged to methyl (A) and methylene (B) carbons of mPEG segments. Notably, small shifts of 'C' and 'D' versus 'B' to higher fields reflected the incorporation of mPEG to PLA via ester bonds. 'E', 'F' and 'G' displayed at 169.31, 68.79 and 16.48 ppm were considered as characteristic peaks of carbonyl, methine and methyl carbons in PLA segments. Similarly, owing to the nucleophilic substitution, peaks at 171.48 ppm (H) was slightly higher than that at 169.31 ppm (E), while peaks at 66.44 ppm (I) was slightly lower than that at 68.79 ppm (F), which were carbonyl and methine carbons, respectively.

FT-NIR spectrum of mPEG-b-PLA copolymer was exhibited in Fig. 1(3). The diblock polymer had two characteristic peaks at 1456.9 and 1111.1 cm^{-1}, which were attributed to asymmetrical and symmetrical stretching vibration ($\nu_{C\text{-}O\text{-}C}$). A strong C-H stretch at 2890.7 cm^{-1} was contributed by both mPEG and PLA segments. A shape stretching vibration of carbonyl groups ($\nu_{C=O}$, 1758.4 cm^{-1}) in PLA segments was also presented.

DSC is widely used to distinguish synthetic polymers and their physical mixture. The plots of mPEG and DL-Lactide with melting points at 125.0 and 51.5 ℃, respectively, were collected in Fig. 1(4, a and b). Interestingly, the calorimetric curve of their physical mixture exhibited a mild endothermic peak at 51.6 ℃ and a sharp endothermic peak at 124.7 ℃, which exactly corresponded to melting points of mPEG and DL-Lactide. Unlike to the physical mixture, mPEG-b-PLA copolymer revealed a strikingly contrasting DSC thermogram, where another endothermic peak without obvious melting peaks of mPEG and DL-Lactide appeared, indicating that the diblock polymer had been successfully synthesized.

Spectra illustration of ITZ-NP

XRPD was used to determine the crystalline or non-crystalline nature of ITZ in lyophilized nanoparticle powder. mPEG-b-PLA copolymer in Fig. 2(1) showed broad humps of amorphous, practically two characteristic diffraction peaks at 19.29° and 23.43°. ITZ powder showed strong typical crystalline diffraction peaks. For the physical mixture of ITZ and mPEG-b-PLA copolymer, broad humps together with characteristic diffraction peaks of the diblock polymer and typical peaks of ITZ were apparently visible. However, for ITZ-NP lyophilized powder, there was no evidence of crystalline characteristics of ITZ and the pattern appeared identical to that of mPEG-b-PLA copolymer, suggesting that ITZ was at an amorphous state in ITZ-NP.

DSC was also utilized to investigate the existing form of ITZ in nanoparticles. In Fig. 2(2), the melting endothermal peak of mPEG-b-PLA copolymer was recorded at 43.8 ℃, while that of bulk ITZ was recorded at 165.7 ℃. Their physical mixture showed both features of diblock polymer and ITZ without variations in peak shapes and their onsets. However, for ITZ-NP, only an endothermal peak of mPEG-b-PLA copolymer at 42.6 ℃ but no peaks of ITZ was found. Since lyophilized products had been stored for one month at 4 ℃ prior to analysis, it could be concluded that ITZ did not exist in ITZ-NP as crystal and had mutual effect with mPEG-b-PLA copolymer.

To validate the interactions between ITZ and mPEG-b-PLA copolymer, FT-NIR analysis was conducted. As illustrated in Fig. 2(3), the specific FT-NIR spectrum of ITZ powder was noticed at 400-1800 cm^{-1}. Characteristic peaks of ITZ at 1700, 1520 and 1230 cm^{-1} were observed in the physical mixture, which could not been observed in ITZ-NP, indicating that there were some interactions between ITZ and mPEG-b-PLA copolymer in ITZ-NP. As was pointed by Yi et al., a polymer–drug complex might form by the reaction

between the carboxyl group of PLA and the amine or triazole group of ITZ [24].

The morphology of ITZ-NP was evaluated by AFM. Those particles displayed compact and close to spherical in shape with a size ranging from 30 to 50 nm, thus a typical core-shell structure formed.

Physicochemical characterization

The reconstituted ITZ-NP solution was light blue in color with opalescence. Drug loading of ITZ-NP was 3.82 ± 0.02 %, while entrapment efficiency was relatively high, 99.40 ± 0.53 %, indicating that mPEG-b-PLA copolymer provided desired solubilization.

The mean diameter and polydispersity index (PDI) of water-dispersed ITZ-NP were also measured, and the data suggested that nanoparticles exhibited a unimodal distribution with an average size of 53.6 ± 0.4 nm (PDI: 0.313 ± 0.015), which was consistent with the measurements made by AFM. What's more, zeta potential of ITZ-NP (-0.17 ± 0.05 mV) belonged to the electric neutrality range. As an inclusion complex, ITZ-HP-β-CD formed a unique molecular shape, and its size cannot be measured accurately by DLS.

The pH values of all ITZ formulations (ITZ-NP: 4.95 ± 0.08; ITZ-HP-β-CD: 4.56 ± 0.12) ranged from 4.50 to 5.00, and the OP values (ITZ-NP: 302.33 ± 2.52; ITZ-HP-β-CD: 381.02 ± 3.01) ranged from 300.00 to 400.00 mOsmol/L, which were considered acceptable to avoid the risk of irritation upon application to veins.

For reconstitution stability test (Table 1), as the concentration of ITZ in ITZ-NP and ITZ-HP-β-CD was diluted below 1 mg/mL, those antifungal drugs would gradually precipitate from the solutions, suggesting that their dilution stability were comparable to each other.

Release profiles and mechanism

In vitro drug release kinetics of ITZ-NP was exhibited in Fig. 3(A). The solubility of ITZ is very low in water. Acidic condition with 0.7% HCl and Tween 80 were used together to prevent free drug precipitating in the dialysis bags. The cumulative release of ITZ during the initial 30 min was 15.23 ± 3.66%. The rest of ITZ in ITZ-NP was continuously released over 16 h. The initial burst release could help the drug delivery system quickly reached the therapeutic concentration, which was quite important for antifungal drugs. On the other hand, even though release profiles of ITZ-NP and ITZ-HP-β-CD were similar and both possessed remarkable sustained release character, the release kinetics of the former was much steadier than that of the later.

In vitro drug release is an important index for nanoparticles to obtain an adapted release for intravenous administration. Therefore, release mechanism was further investigated. Table 2 showed the fitting equations and their corresponding correlation coefficients. Correlation coefficients confirmed that release mechanism of ITZ-NP was better described by the Peppas-Sahlin model. The R^2 value was 0.9972, which indicated that release mechanism was non-Fickian, but followed the coupled Fick-Erosion diffusion mechanism. Respective contribution from Fick or Erosion was exhibited in Fig. 3(B). Fick diffusion occupied a predominant position during the whole period, however, prolonging release time resulted in a slight decrease of its proportion. Erosion had limited effect on drug release, even its proportion tended to modestly increase as time went on. Thus, it was believed that ITZ was entrapped in mPEG-b-PLA copolymer and mostly released from drug reservoirs by Fick diffusion. In addition, due to the permeation of release medium, the cores of nanoparticles expanded, which also led to drug release and was recognized as Erosion mechanism.

Antifungal activity assay

In vitro antifungal activity of different ITZ formulations was investigated against *C. albicans*. The efficiency of the prepared ITZ delivery system was compared with commercial preparation. ITZ concentrations ranged from 0.0153 to 1000.0000 μg/mL were selected on the basis of preliminary data using Sabouraud's Glucose Agar Plate [25]. As seen from Fig. 4, ITZ-NP and ITZ-HP-β-CD presented comparable inhibition rates to *C. albicans*, with ITZ-NP being slightly more potent across all the tested concentration ranges, which may be attributed to the effect of nanoparticles on the cell wall of the microorganism. At the initial concentration of 0.0153 μg/mL, the antifungal effect of ITZ-NP (28.9902%) was almost two times as high as that of ITZ-HP-β-CD (14.0065%), suggesting that the nanoparticle formulation preserved its strong inhibition in fungal growth especially at low ITZ levels.

Biocompatibility

Hemolytic potentials of ITZ formulations were evaluated with rabbit blood to ensure their hemocompatibility. mPEG-b-PLA copolymer was dosed at corresponding concentrations which were equivalent to their contents in ITZ-NP, and the concentrations of Tween 80 were equivalent to that of mPEG-b-PLA copolymer. Hemolysis ratios were quantified based on spectrophotometric measurements of hemoglobin released from RBCs and results were presented in Fig. 5. When the concentrations of ITZ were less than 1 mg/mL, hemolysis ratios of ITZ-NP and mPEG-b-PLA copolymer were lower than 5%, indicating qualified hemocompatibility. In contrast, as the concentrations of ITZ increased above 0.1 mg/mL, ITZ-HP-β-CD had significant leakage of hemoglobin, similar to those of Tween 80. Thus, it could be concluded that ITZ-NP were more biocompatible than ITZ-HP-β-CD because of milder hemolysis.

The visual examination of rabbit ear veins was executed by a designated bystander after each administration of ITZ formulations. Severe venous irritation was recorded in ITZ-HP-β-CD group since the second injection, including vascular engorgement, dropsy, discoloration, induration, etc. On the contrary, slight venous irritation was noted in ITZ-NP group and no obvious visible damages around injection sites were found in the other two groups.

Subsequently, rabbit ears were sectioned and stained with HE. Fig. 6 showed microscopic examination of marginal ear veins after injection with different sample solutions.

Physiological saline group served as a control for changes rooted from mechanical punctuation during injection. In ITZ-HP-β-CD group, serious injection irritation, such as destruction of vascular wall, anapetia and congestion of blood vessel, edema, bleeding and inflammatory cell infiltration of peritubular tissues, was captured in most regions, even distant from injection sites, while similar phenomena were hardly observed in mPEG-b-PLA copolymer and ITZ-NP group. Thus it could be concluded that nanoscale ITZ-NP would produce much less injection irritation than ITZ-HP-β-CD.

Tissue distribution and pharmacokinetics

After i.v. bolus injection of ITZ formulations to mice, the average drug concentration of plasma and major organs vs. time profiles were plotted in Fig. 7. ITZ concentrations in different tissues all exhibited successive decrease with time. Importantly, at most indicated times, in the plasma, liver and spleen, ITZ levels for the group treated with ITZ-NP were significantly higher than those for the group treated with ITZ-HP-β-CD, which might be the dramatic increase of particle size. While for other organs, such as heart, lung, kidney and brain, noticeable decrease of ITZ contents was found after administration of ITZ-NP. Thus, the altered tissue distribution of ITZ-NP (versus ITZ-HP-β-CD) was responsible for enhancement of bioavailability and alleviation of serious reactions to major organs, especially heart and kidney.

Meanwhile, all pharmacokinetic parameters were analyzed by non-compartmental model and listed in Table 3. To represent targeting ability, Re, Te, R_{Te} and Ce were calculated and collected in Table 4. Dramatic changes of distribution could be observed between ITZ-NP and ITZ-HP-β-CD after intravenous administration.

According to above definition of Re, if its value exceeded 1, the tissue was deemed to expose to ITZ to a greater extent by nanoparticles. As expected, Re for plasma was 1.334, obviously higher compared with other tissues, demonstrating that the retardation of ITZ in blood circulation was significantly increased, which was ascribed to the protection of core-shell structure and slow drug release from nanoparticles. Besides, Re for liver and spleen were also higher than 1, which indicated that ITZ-NP was also inclined to distribute to liver and spleen though less preferable to plasma. Reticuloendothelial system (RES) might be responsible for the accumulation in liver and spleen [26-29]. Some fungi, such as Histoplasma, readily spreads in macrophages throughout the RES [30]. The retention of ITZ in RES might be helpful for the therapy of Histoplasmosis. All these results indicated that the encapsulation of ITZ in large-sized nanoparticles induced long retention in systemic circulation and partial uptake by RES.

Although Re is a good indicator about the relative efficacy of two delivery systems in reference to one tissue, it cannot provide any information regarding the efficacy of a given delivery system. Hence, Te was introduced to demonstrate the selectivity of a delivery system against the specific tissue. A greater Te typified a higher selectivity of a given tissues and R_{Te} represented the increase in the times of nanoparticle targeting efficiency compared with cyclodextrin inclusion compounds. As seen in Table 4, total Te values of ITZ-NP (72%) to plasma, liver and spleen elevated significantly compared with ITZ-HP-β-CD (53.4%). Moreover, only in plasma, liver and spleen, R_{Te} exceeded 1, indicating that targeting efficiency of ITZ-NP to blood and RES-rich organs was really higher.

Ce represents the change in the extent of a delivery system on biodistribution. According to calculation, Ce in plasma and spleen increased by factors of 1.053 and 1.500 compared with ITZ-HP-β-CD in the case of ITZ-loaded mPEG-b-PLA nanoparticles, and Ce in brain also increased by a factor of 1.124, whereas Ce in kidney, heart, lung and liver decreased differently, indicating that the developed nanoparticles resulted in an obvious change in tissue distribution. This might be helpful to decrease possible toxicity of these sites, *e.g.*, lowering the side effect of kidney and heart caused by the administration of HP-β-CD [31].

These results confirmed that ITZ-NP with long circulation time could preferably bypass both renal clearance and heart entrapment due to their desirable size, thus had a potential to enhance the efficacy in treating fungal infection and decrease side effects of non-targeting sites.

Conclusions

To sum up, ITZ was successfully enveloped in mPEG-b-PLA nanoparticles using film dispersion method. ^{1}H NMR, ^{13}C NMR, FT-NIR and DSC spectra verified ring-opening polymerization of mPEG-b-PLA copolymer. XRPD, DSC and FT-NIR measurements revealed that ITZ existed as amorphous in ITZ-NP and interacted with mPEG-b-PLA copolymer. ITZ-NP had diameters of 53.6 nm with narrow polydispersity and exhibited acceptable physical properties. *In vitro* release showed that ITZ-NP exhibited sustained release after an initial burst release. In spite of that, the antifungal activity of ITZ-loaded nanoparticles remained as potent as ITZ-HP-β-CD. Hemolysis and vascular stimulation further confirmed that ITZ-NP was more biocompatible than marketed ITZ-HP-β-CD formulation. *In vivo* fate of ITZ was evaluated after intravenous administration of ITZ-NP and ITZ-HP-β-CD. Compared with the ITZ-HP-β-CD, ITZ-NP achieved a prolonged circulation time and improved the overall targeting ability to RES-rich organs. With respect to these observations, it can be concluded that mPEG-b-PLA nanoparticles may be a promising carrier for intravenous delivery of ITZ.

Acknowledgements

The authors report no declarations of interest. This work was funded by the National Natural Science Foundation of China

(NO. 81501579), the Natural Science Foundation of Jiangsu Province (NO. BK20150702), and the Priority Academic Program Development of Jiangsu Higher Education Institutions. The authors also acknowledge Baoqiang Tang and Ershuang Yang for their kind assistance in experimental operation.

Notes and references

1 O. Lortholary, D. W. Denning and B. Dupont, *J. Antimicrob. Chemother.*, 1999, **43**, 321-331.
2 S. M. Grant and S. P. Clissold, *Drugs*, 1989, **37**, 310-344.
3 H. Van Cauteren, J. Heykants, R. De Coster and G. Cauwenbergh, *Rev. Infect. Dis.*, 1987, **9 Suppl 1**, S43-46.
4 J. E. Edwards, Jr., G. P. Bodey, R. A. Bowden, T. Buchner, B. E. de Pauw, S. G. Filler, M. A. Ghannoum, M. Glauser, R. Herbrecht, C. A. Kauffman, S. Kohno, P. Martino, F. Meunier, T. Mori, M. A. Pfaller, J. H. Rex, T. R. Rogers, R. H. Rubin, J. Solomkin, C. Viscoli, T. J. Walsh and M. White, *Clin. Infect. Dis.*, 1997, **25**, 43-59.
5 D. J. Sheehan, C. A. Hitchcock and C. M. Sibley, *Clin. Microbiol. Rev.*, 1999, **12**, 40-79.
6 J. H. Rex, M. A. Pfaller, J. N. Galgiani, M. S. Bartlett, A. Espinel-Ingroff, M. A. Ghannoum, M. Lancaster, F. C. Odds, M. G. Rinaldi, T. J. Walsh and A. L. Barry, *Clin. Infect. Dis.*, 1997, **24**, 235-247.
7 W. S. Zheng, X. Q. Fang, L. L. Wang and Y. J. Zhang, *Int J Pharm*, 2012, **436**, 291-298.
8 J. Peeters, P. Neeskens, J. P. Tollenaere, P. Van Remoortere and M. E. Brewster, *J. Pharm. Sci.*, 2002, **91**, 1414-1422.
9 M. Van Speybroeck, R. Mols, R. Mellaerts, T. D. Thi, J. A. Martens, J. Van Humbeeck, P. Annaert, G. Van den Mooter and P. Augustijns, *Eur. J. Pharm. Biopharm.*, 2010, **75**, 354-365.
10 P. D. R. Thomson and N. J. Montvale, *Physicians' Desk Reference*, 59 edn., 2005, pp. 1757-1766.
11 G. S. Kwon and T. Okano, *Advanced Drug Delivery Reviews*, 1996, **21**, 107-116.
12 O. C. Farokhzad and R. Langer, *ACS Nano*, 2009, **3**, 16-20.
13 W. Sun, Y. Lu and Z. Gu, *Particle & Particle Systems Characterization*, 2014, **31**, 1204-1222.
14 R. Langer and D. A. Tirrell, *Nature*, 2004, **428**, 487-492.
15 S. Singh and S. S. Ray, *J. Nanosci. Nanotechnol.*, 2007, **7**, 2596-2615.
16 C. Li, Y. Shen, C. Sun, C. Nihad and J. Tu, *Drug Deliv.*, 2015, **0**, 1-8.
17 J. Shi, J. Zhang, Y. Shen, L. Tang, J. Zhao, J. Tu, Y. Tian and Y. Feng, *Drug Deliv.*, 2015, **22**, 168-181.
18 X. Zheng, B. Kan, M. Gou, S. Fu, J. Zhang, K. Men, L. Chen, F. Luo, Y. Zhao, X. Zhao, Y. Wei and Z. Qian, *Int J Pharm*, 2010, **386**, 262-267.
19 Y. Shen, X. Ling, W. Jiang, S. Du, Y. Lu and J. Tu, *Drug Deliv.*, 2015, **22**, 911-917.
20 R. K. O'Leary and W. L. Guess, *J. Pharm. Sci.*, 1968, **57**, 12-17.
21 J. B. Gordien, A. Pigneux, S. Vigouroux, R. Tabrizi, I. Accoceberry, J. M. Bernadou, A. Rouault, M. C. Saux and D. Breilh, *J. Pharm. Biomed. Anal.*, 2009, **50**, 932-938.
22 L. H. Luo, P. J. Zheng, H. Nie, Y. C. Chen, D. Tong, J. Chen and Y. Cheng, *Drug Deliv.*, 2015, DOI: 10.3109/10717544.2014.980525, 1-9.
23 S. Y. Kim, I. G. Shin and Y. M. Lee, *Journal of Controlled Release*, 1998, **56**, 197-208.
24 Y. Yi, H. J. Yoon, B. O. Kim, M. Shim, S. O. Kim, S. J. Hwang and M. H. Seo, *J Control Release*, 2007, **117**, 59-67.
25 A. H. Alomrani, G. A. Shazly, A. A. Amara and M. M. Badran, *Colloids Surf. B Biointerfaces*, 2014, **121**, 74-81.
26 L. Grislain, P. Couvreur, V. Lenaerts, M. Roland, D. Deprez-Decampeneere and P. Speiser, *International Journal of Pharmaceutics*, 1983, **15**, 335-345.
27 Y. Chikamasa, M. Hirotami, A. Kazue and K. Hiroshi, *International Journal of Pharmaceutics*, 1991, **70**, 225-233.
28 X. Ling, Y. Shen, R. Sun, M. Zhang, C. Li, J. Mao, J. Xing, C. Sun and J. Tu, *Polym. Chem.*, 2015, **6**, 1541-1552.
29 A. Balducci, Y. Wen, Y. Zhang, B. M. Helfer, T. K. Hitchens, W. S. Meng, A. K. Wesa and J. M. Janjic, *Oncoimmunology*, 2013, **2**, e23034.
30 C. A. Kauffman, *Clin. Chest Med.*, 2009, **30**, 217-225, v.
31 S. Gould and R. C. Scott, *Food Chem. Toxicol.*, 2005, **43**, 1451-1459.

Journal Name

ARTICLE

Tables:

Table 1 Dilution stability of ITZ formulations.

Concentration (mg/mL)	ITZ-NP in10% FBS DMEM media	ITZ-HP-β-CD in 10% FBS DMEM media
3	No drug precipitation	No drug precipitation
1	Drug precipitation	Drug precipitation
0.066	Drug precipitation	Drug precipitation

Table 2 Fitting equations and correlation coefficients.

Model	Equation	Correlation coefficient (R^2)
Zero-order	$Q = 0.092\ t$	0.7266
Higuchi	$Q = 0.270\ t^{0.5}$	0.9839
Weibull	$Q = 100\ \{1 - Exp[-\ (t - 0.207)^{0.460} / 331.965]\}$.	0.9942
Peppas-Sahlin	$Q = 0.268\ t^{0.719} - 0.020\ t^{1.438}$	0.9972

Table 3 Pharmacokinetic parameters of ITZ formulations. Data are represented as mean ± SD from six independent experiments.

Samples	C_{max} (μg/mL or μg/g)		V_{ss} (L)		Cl (L/h)		$AUC_{0\text{-}inf}$ (h·μg/mL or h·μg/g)		$AUMC_{0\text{-}inf}$ (h^2·μg/mL or h^2·μg/g)		$MRT_{0\text{-}inf}$ (h)	
	ITZ-NP	ITZ-HP-β-CD	ITZ-NP	ITZ-HP-β-CD	ITZ-NP	ITZ-HP-β-CD	ITZ-NP	ITZ-HP-β-CD	ITZ-NP	ITZ-HP-β-CD	ITZ-NP	ITZ-HP-β-CD
Plasma	10.017 ± 0.720	9.511 ± 1.880	2.220 ± 0.212	3.598 ± 1.109	0.968 ± 0.263	1.291 ± 0.202	20.656 ± 2.124	15.487 ± 3.111	47.353 ± 6.128	43.154 ± 6.442	2.292 ± 1.123	2.786 ± 1.090
Heart	1.636 ± 0.840	2.483 ± 1.320	22.069 ± 4.391	43.129 ± 3.975	4.626 ± 2.712	1.593 ± 0.304	4.324 ± 1.027	12.556 ± 3.192	20.629 ± 4.737	339.980 ± 12.039	4.771 ± 2.127	27.077 ± 7.889
Liver	13.267± 2.521	14.035 ± 1.501	3.417 ± 1.103	4.859 ± 1.928	1.052 ± 0.229	1.090 ± 0.574	19.017 ± 2.792	18.353 ± 3.553	61.782 ± 8.993	81.836 ± 10.211	3.249 ± 1.108	4.459 ± 3.093
Spleen	1.963 ± 0.621	1.309 ± 0.955	8.253 ± 2.506	9.814 ± 2.017	15.056 ± 2.384	18.771 ± 1.153	1.328 ± 0.627	1.065 ± 0.022	0.728 ± 0.120	0.557 ± 0.119	0.548 ± 0.295	0.523 ± 0.205
Lung	1.425 ± 0.992	1.684 ± 0.831	5.523 ± 2.783	23.669 ± 4.947	5.783 ± 1.134	2.846 ± 0.128	3.458 ± 1.992	7.026 ± 1.207	3.303 ± 1.097	58.429 ± 9.749	0.955 ± 0.404	8.316 ± 3.491
Kidney	1.029 ± 0.811	1.597 ± 1.230	10.864 ± 2.686	10.790 ± 2.647	32.393 ± 5.228	18.868 ± 3.782	0.617 ± 0.301	1.060 ± 0.501	0.207 ± 0.100	0.606 ± 0.299	0.335 ± 0.222	0.572 ± 0.221
Brain	5.709 ± 1.531	5.078 ± 1.490	7.064 ± 3.004	7.377 ± 1.190	2.553 ± 1.001	2.036 ± 0.628	7.834 ± 3.191	9.822 ± 0.309	21.674 ± 5.297	35.583 ± 12.029	2.767 ± 1.044	3.623 ± 1.006

Table 4 Target parameters of ITZ formulations after an intravenous administration in mice.

Samples	Re	Te		R_{Te}	Ce
		ITZ-NP	ITZ-HP-β-CD		
Plasma	1.334	36.5%	23.7%	1.523	1.053

Heart	0.344	7.6%	19.2%	0.393	0.659
Liver	1.036	33.2%	28.1%	1.183	0.945
Spleen	1.247	2.3%	1.6%	1.424	1.500
Lung	0.492	6.0%	10.7%	0.562	0.846
Kidney	0.582	1.1%	1.6%	0.665	0.645
Brain	0.798	13.7%	15.0%	0.911	1.124

Captions:

Fig. 1 (1) ^{1}H NMR, (2) ^{13}C NMR and (3) FT-NIR spectra of mPEG-b-PLA copolymer. (4) DSC spectra of (a) mPEG 2000, (b) DL-Lactide, (c) the physical mixture of mPEG 2000 and DL-Lactide at a weight ratio of 40:60, (d) mPEG-b-PLA copolymer at a block ratio of 40:60.

Fig. 2 (1) XRD patterns, (2) DSC and (3) FT-NIR spectra of (a) mPEG-b-PLA copolymer, (b) ITZ, (c) the physical mixture of ITZ and mPEG-b-PLA copolymer at a weight ratio of 1:25, (d) ITZ-NP at a weight ratio of 1:25. (4) AFM images of ITZ-NP at an optimal dilution ratio.

Fig. 3 (A) Cumulative release profiles of ITZ from ITZ formulations. (B) The percentage of Fick diffusion and Erosion during drug released from ITZ-NP.

Fig. 4 Inhibition rate of ITZ formulations against *C. albicans*.

Fig. 5 Hemolysis results of ITZ-HP-β-CD, ITZ-NP, mPEG-b-PLA copolymer and Tween 80, where the hemolysis values of positive control (distilled water) and negative control (physiological saline) were 100% and 0%.

Fig. 6 Histopathological examination of rabbit ear-rim auricular veins following different injections: (A) physiological saline; (B) mPEG-b-PLA copolymer; (C) ITZ-NP and (D) ITZ-HP-β-CD.

Fig. 7 Biodistribution of ITZ in plasma, heart, liver, spleen, lung, kidney and brain after an intravenous administration of ITZ formulations.

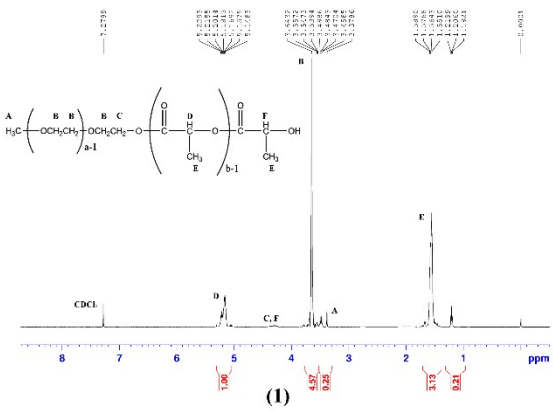

(1)

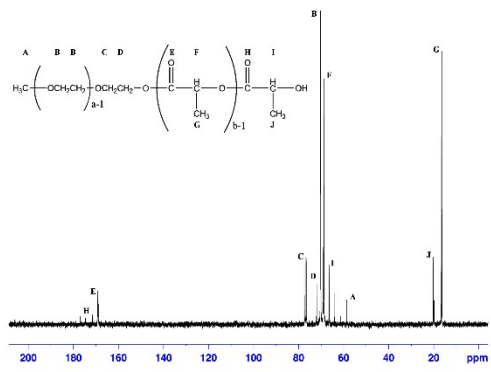

(2)

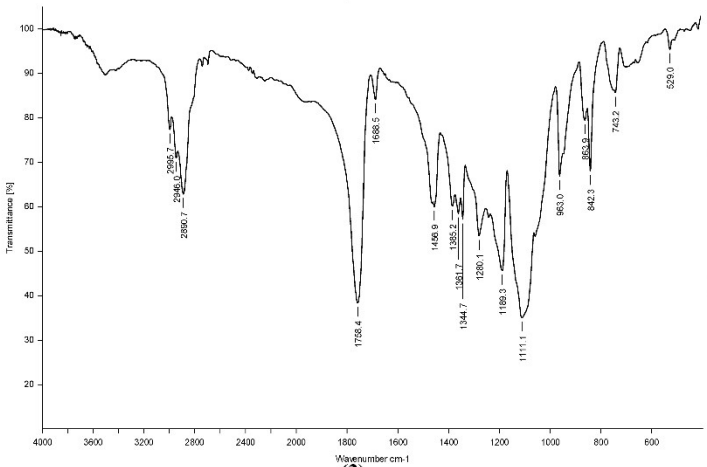

(3)

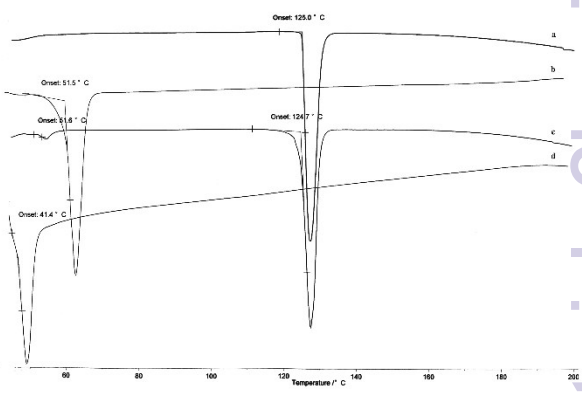

(4)

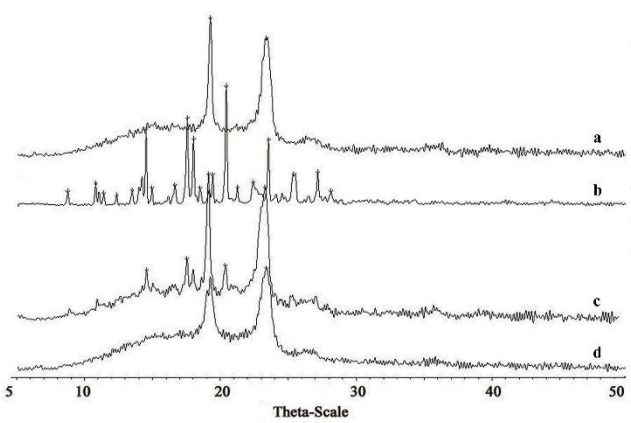

(1)

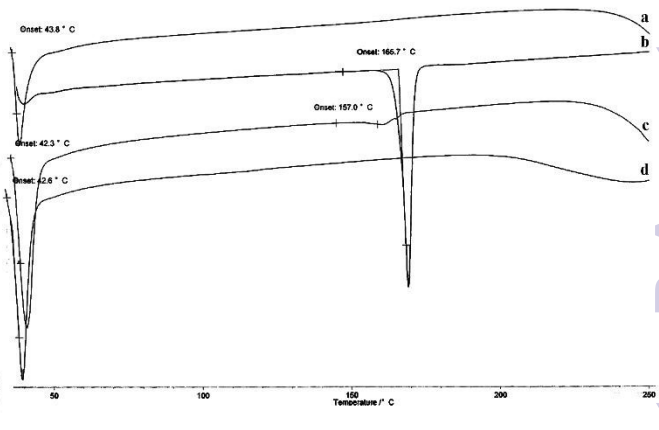

(2)

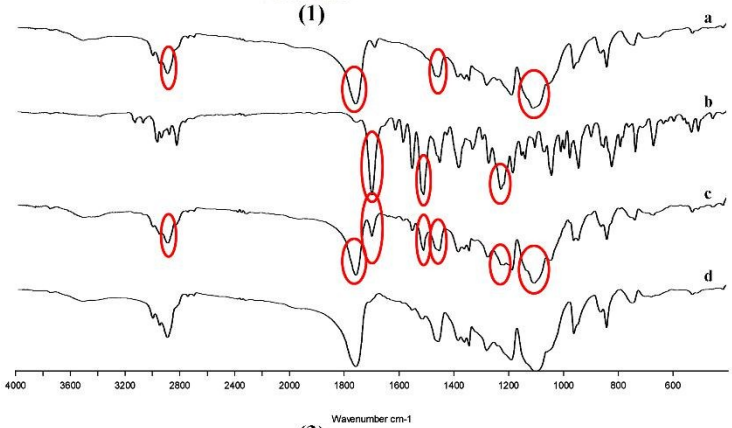

(3)

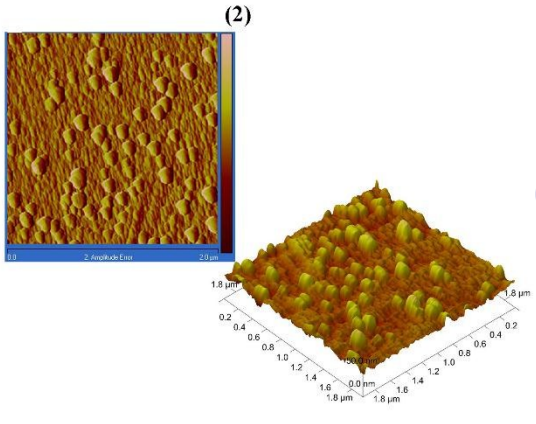

(4)

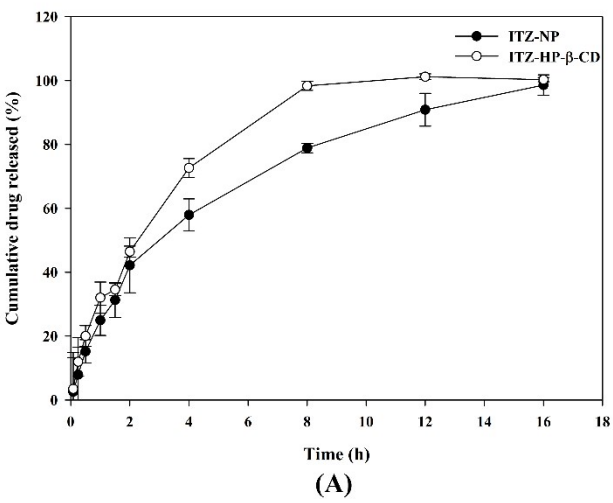

(A)

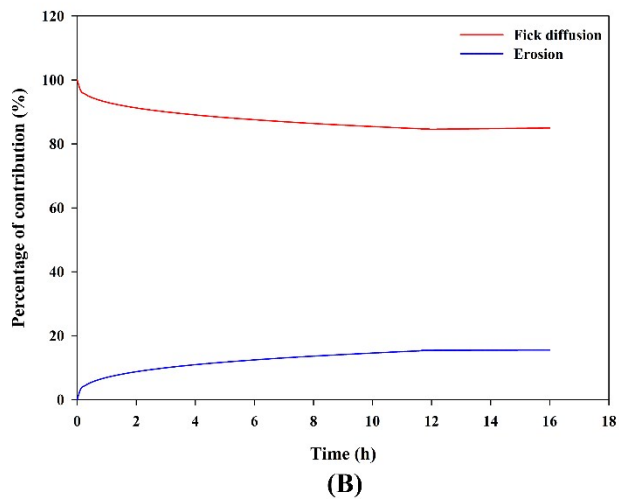

(B)

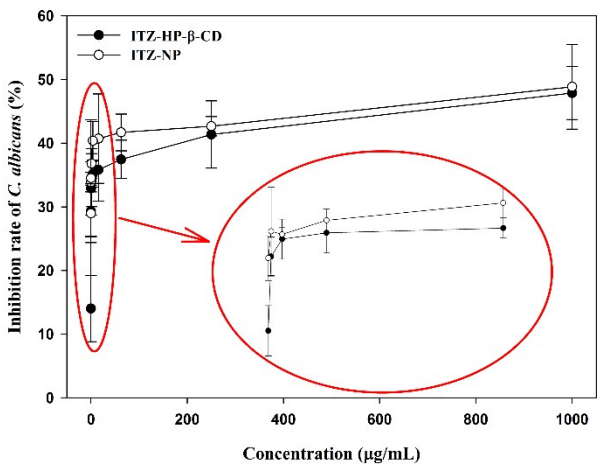

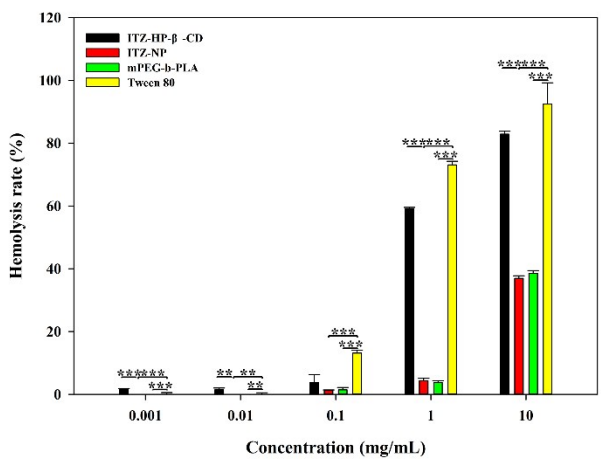

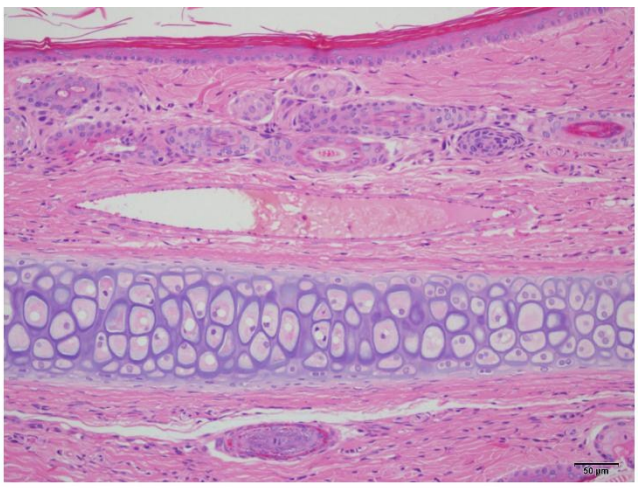

(A)

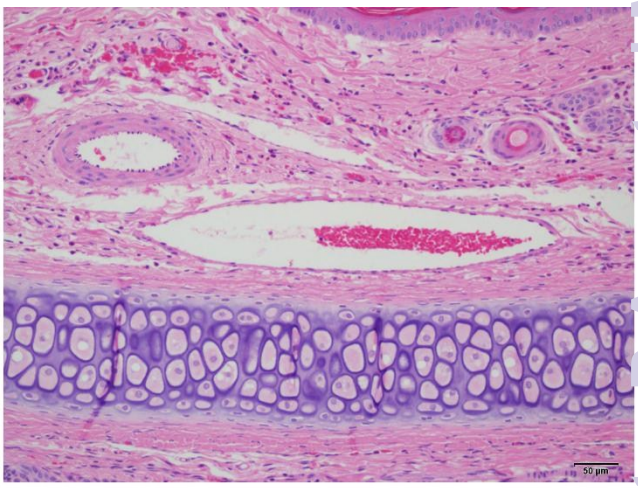

(B)

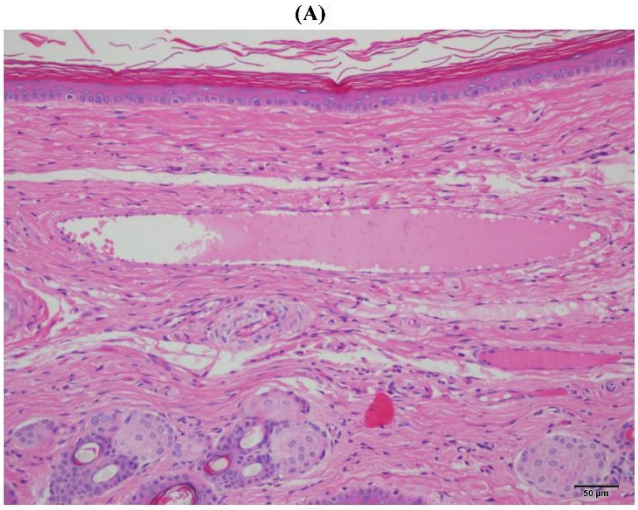

(C)

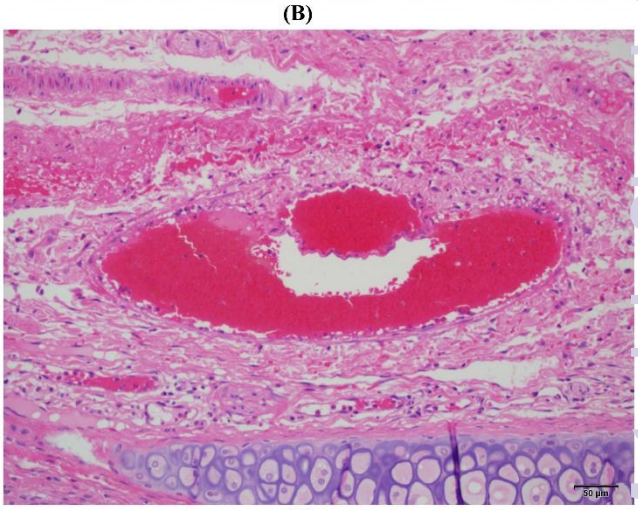

(D)

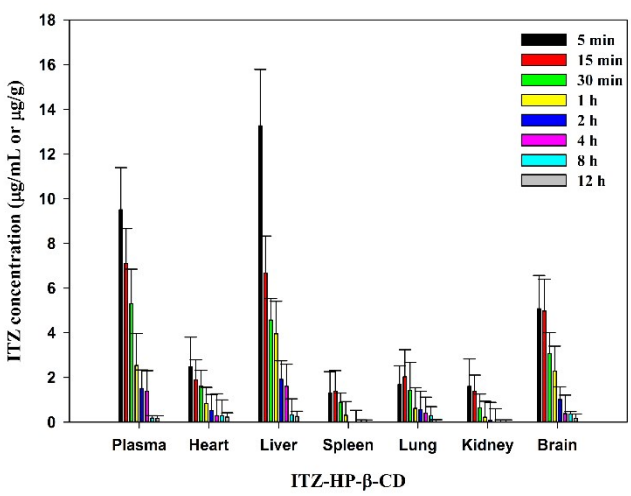

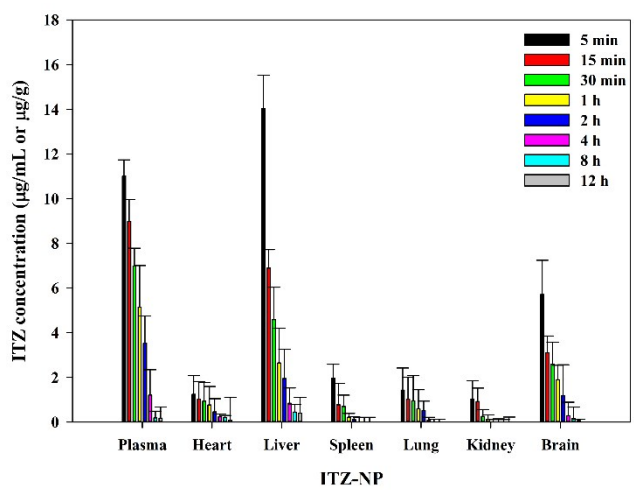

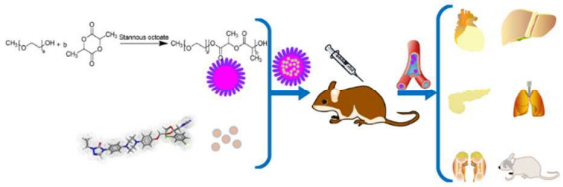

Schematic illustration for construction and *in vivo* trafficking of ITZ-NP.